Available online at www.sciencedirect.com

ScienceDirect

Solar Energy 96 (2013) 159–167

SOLAR ENERGY

www.elsevier.com/locate/solener

Properties of a general azimuth–elevation tracking angle formula for a heliostat with a mirror-pivot offset and other angular errors

Minghuan Guo, Feihu Sun, Zhifeng Wang *, Jianhan Zhang

Key Laboratory of Solar Thermal Energy and Photovoltaic System of Chinese Academy of Sciences, Institute of Electrical Engineering, Beijing 100190, China

Received 30 January 2013; received in revised form 18 June 2013; accepted 29 June 2013
Available online 9 August 2013

Communicated by: Associate Editor Lorin Vant-Hull

Abstract

The solar field of a central receiver system (CRS) is an array of dual-axis tracking heliostats on the ground beside or around a central tower, with each heliostat tracking the sun to continuously reflect the solar beam onto the fixed tower-top receiver. Azimuth–elevation tracking (also called altitude–azimuth tracking) is the most common and popular tracking methods used for heliostats. A general azimuth–elevation tracking angle formula was developed previously for a heliostat with a mirror-pivot offset and other typical geometric errors. The angular error parameters in this tracking angle formula are the tilt angle, ψ_t, and the tilt azimuth angle, ψ_a, for the azimuth axis from the vertical direction, the dual-axis non-orthogonal angle, τ_1 (bias angle of the elevation axis from the orthogonal to the azimuth axis), and the non-parallel degree, μ, between the mirror surface plane and the elevation axis (canting angle of the mirror surface plane relative to the elevation axis). This tracking angle formula is re-rewritten here as a series of easily solved expressions. A more numerically stable expression for the mirror-center normal is then presented that is more useful than the original mirror–normal expression in the tracking angle formula. This paper discusses some important angular parametric properties of this tracking angle formula. This paper also gives an approach to evaluate the tracking accuracy around each helistat rotational axis from experimental tracking data using this general tracking angle formula. This approach can also be used to determine the heliostat zero angle positioning errors of the two rotational axes. These supplementary notes make the general azimuth–elevation tracking angle formula more useful and effective in solar field tracking designs.

Keywords: Heliostat; Azimuth–elevation tracking; Tracking angle formula; Mirror-pivot offset

1. Introduction

Various dual-axis tracking modes have been listed in literature (Lipps and Vant-Hull, 1978), such as altitude–azimuth (also called azimuth–elevation), radial pitch-roll, azimuth pitch-roll, polar and receiver oriented tracking methods. Guo et al. (2010) gave an overview of the dual-axis tracking modes and the geometric characteristics of these tracking modes. As the heliostat tracks the sun, the mirror normal is guided to the half angle direction between the sun direction and the aim point direction, so that the incident sun beam on the mirror surface center is reflected to the aim point. Of all the dual-axis tracking modes, the azimuth–elevation tracking mode is the most popular for heliostats. For an azimuth–elevation tracking heliostat, the primary axis is the azimuth axis which is fixed to the ground plane pointing towards the zenith. The secondary axis is the elevation axis which is rotating together with the mirror surface around the azimuth axis.

However, real azimuth–elevation tracking heliostats always have geometric errors due to mechanism imperfections. Baheti and Scott (1980) identified several physical

* Corresponding author. Tel.: +86 10 62520684; fax: +86 10 62587946.
E-mail addresses: minghuan_guo@163.com (M. Guo), zhifeng@vip.sina.com (Z. Wang).

0038-092X/$ - see front matter © 2013 Elsevier Ltd. All rights reserved.
http://dx.doi.org/10.1016/j.solener.2013.06.031

factors that contribute to tracking errors of a dual-axis solar tracker (not a heliostat), which are pedestal tilt, azimuth and elevation reference biases, and linear gear ratio errors in the azimuth and elevation axes. Mavis (1988) presented studies to characterize the heliostat beam and tracking performance of the Solar One central receiver plant. He identified the potential physical factors contributing to heliostat tracking errors, which included pedestal tilt, non-orthogonality between the elevation and azimuth axes, mirror canting errors, encoder resolution and bias errors of the elevation and azimuth axes, errors in the surveyed heliostat location, and gravity loading and structure deformation. Stone (1986) applied for a US patent entitled "Automatic Heliostat Track Alignment Method" based on a geometric error calibration model where the calibration tracking angles had to be computed iteratively. Stone and Jones (1999) described many tracking error sources, including the three dominant geometric error sources being the azimuth axis tilt error (also called the pedestal tilt error), the mirror canting error and the encoder reference errors, and their effects on heliostat tracking. However, they did not publish the related azimuth–elevation tracking angle algorithm in this document. The derivation of Baheti and Scott's tracking error calibration formulation was extended to a reflected beam model for an azimuth–elevation tracking heliostat (as opposed to on-axis tracking of the sun) with the two error parameters for the drive-axis non-orthogonality and mirror canting errors appended to the original formulation, giving a total of eight error parameters that are needed to automatically correct the heliostat tracking errors (Khalsa et al., 2011). The calibration tracking angles were also determined iteratively. Although Chong and Wong (2009) presented a general formula for an on-axis sun-tracking system with three additional angular parameters, their model only compensated for the dual-axis tracking effect of the azimuth axis tilt error for a sun tracker and was limited to the most common and simple solar altitude angle, α_s, and solar azimuth angle, γ_s, (in the north-to-east direction) given by:

$$\alpha_s = \arcsin(\sin\delta\sin\Phi + \cos\delta\cos\omega\cos\Phi)$$

$$\gamma_s = 180^\circ + sign(\sin\omega)\arccos\left(\frac{\sin\alpha\sin\Phi - \sin\delta}{\cos\alpha\cos\Phi}\right)$$

where Φ is the site latitude (northward is positive), ω is the solar hour angle, and δ is the solar declination. ω and δ are computed using the expressions in the book by Duffie and Beckman (1991).

In practice, there is normally some offset between the mirror surface plane and the heliostat pivot. The heliostat pivot is defined as the intersection of the two rotational axes of the heliostat and the heliostat pivots around this point. The mirror-pivot offset is the perpendicular distance from the heliostat pivot to the mirror surface plane. However, there are no known exact azimuth–elevation tracking angle formulas available for a heliostat that account for the mirror–pivot offset. The difficulty in deriving the exact tracking formulas for the heliostat with a mirror–pivot offset is that the mirror surface center is always moving during sun tracking. As implied by Guo et al. (2010), the exact tracking angle expressions for a receiver oriented spinning–elevation tracking heliostat with a mirror–pivot offset can be solved from a quartic algebraic equation. Since the analytic solution of a quartic equation is complex, the numerical solutions of the quartic are often used in engineering problems. Guo et al. (2010) made a high accuracy approximation to the exact elevation tracking angle correction formulated by the quartic equation, and gave accurate tracking angle formulas to calibrate the effect of the mirror–pivot offset for a standard receiver oriented heliostat assuming that the two rotational axes were orthogonal and the secondary axis was parallel to the mirror surface plane. If the mirror surface center is defined as the orthogonal projection of the heliostat pivot on the mirror surface plane, then the mirror-pivot offset is equal to the distance between the heliostat pivot and the mirror surface center, and the line connecting the heliostat pivot and the mirror surface center always coincides with the mirror-surface-center normal. An accurate mirror normal at the mirror surface center for a heliostat with a mirror-pivot offset was given by Guo et al. (2011). The accurate mirror-surface-center normal expression was then used to develop a general azimuth–elevation tracking angle formula for a heliostat with a mirror-pivot offset and other angular errors (Guo et al., 2011). Fig. 1 shows the geometry for this general azimuth–elevation tracking angle formula. In Fig. 1, θ^* is the incident angle of the sun beam at the mirror surface center **M**, point **O** is the heliostat pivot with vectors **OT**, **ON**,**OS** being the vectors pointing to the aim point **T**, the mirror-surface-center normal and the solar vector. $\vec{t}$,, $\vec{n}$, $\vec{s}$ are the unit vectors for **OT**, **ON** and **OS**, respectively. Π_1 is the dual-axis plane containing the azimuth axis and the elevation axis, while Π_2 is the plane determined by the elevation axis and the mirror surface center **M**. $\mathbf{\Pi_1}$ rotates around the azimuth axis. Π_2 also includes vectors **OS**,**ON** and**OT**. The intersection of Π_1 and Π_2 is the line of elevation axis. The left-handed rotational direction is positive for the azimuth axis, while the right-handed rotational direction is positive for the elevation axis. In this general azimuth–elevation tracking angle formula, the elevation tracking angle is α, the azimuth tracking angle is γ, and the mirror-pivot offset is $\|\mathbf{OM}\| = H_z$. Here, operator $\|\cdot\|$ indicates the magnitude of a vector. The four angular parameters are the tilt angle, ψ_t, and the tilt azimuth angle, ψ_a, of the azimuth axis, the dual-axis non-orthogonal angle, τ_1 (bias angle of the elevation axis from the orthogonal to the azimuth axis), and the canting angle, μ, of the mirror surface plane relative to and along the elevation axis. Here, the mirror canting error does not refer to the canting of the mirror facets, but to the bias of the mirror-surface-center normal from the expected

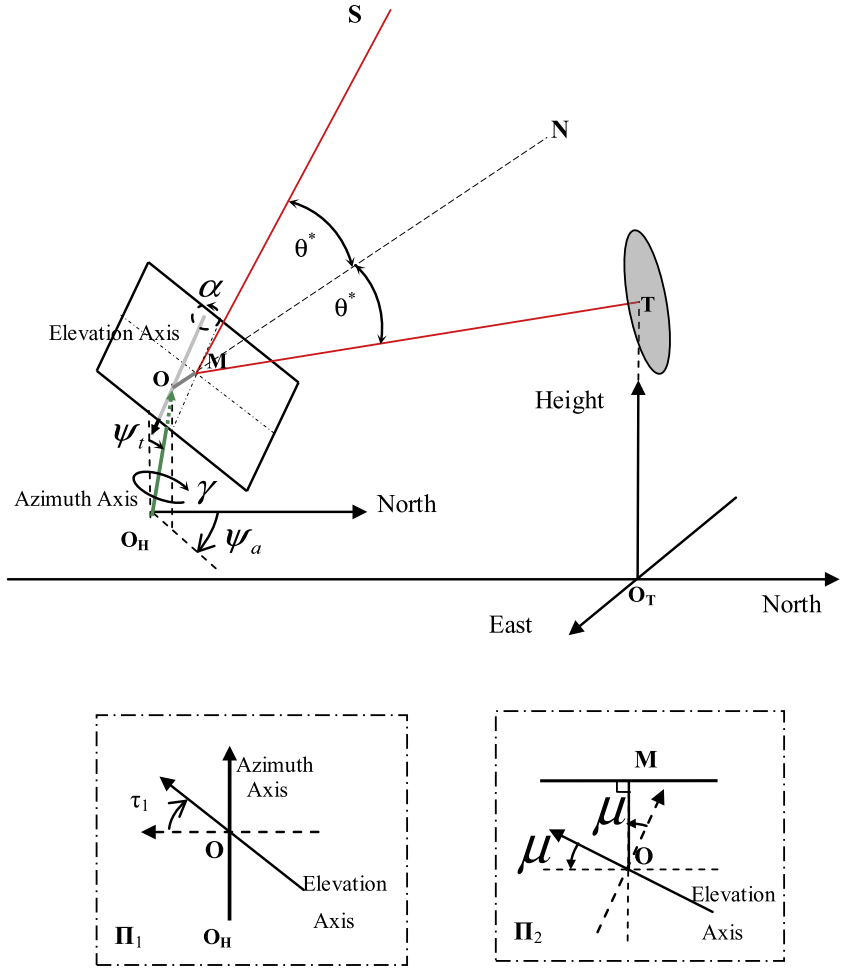

Fig. 1. Azimuth–elevation tracking geometry for a heliostat with a mirror-pivot offset and angular tracking parameters. The upper part is the 3D plot of the heliostat tracking geometry, while the lower part shows 2D plots of planes Π_1 and Π_2 marked at the boundaries by dashed and dotted lines.

direction. Since the around-elevation-axis angular component of the mirror-surface-center normal is indistinguishable from an elevation-axis encoder reference error, the mirror canting angle here is interpreted as the non-parallel degree of the entire mirror surface plane relative to the elevation axis. An encoder reference error just causes a shift of the tracking angle around the rotational axis, so the encoder reference errors are not included in this tracking angle formula. When $\psi_t = 0°$, $\tau_1 = 0°$, $\mu = 0°$, $\gamma = 0°$ and $\alpha = 0°$, the heliostat is in the vertical position with the mirror-surface-center normal $\vec{n}$, horizontal and pointing exactly north, i.e. $\vec{n}, = (1, 0, 0)$ in a left-handed Cartesian coordinate system [**O**; North, East, Height].

For the current solar altitude angle, α_s, and the current solar azimuth angle, γ_s, (in the north-to-east direction), the accurate mirror normal can be expressed as (Guo et al., 2011):

$$\vec{s} = (s_1, s_2, s_3) = (\cos\alpha_s \cos\gamma_s, \cos\alpha_s \sin\gamma_s, \sin\alpha_s) \quad (1)$$

$$L = \|\mathbf{OT}\| = \|(t_1, t_2, t_3)\| = \sqrt{t_1^2 + t_2^2 + t_3^2} \quad (2)$$

$$\vec{t} = \mathbf{OT}/L \quad (3)$$

$$\theta = 0.5 \cdot \cos^{-1}(\vec{s} \cdot \vec{t}) \quad (4)$$

$$\tau = \sin^{-1}\left(\frac{H_z \sin\theta}{2L - H_z \cos\theta}\right) \quad (5)$$

$$\theta' = \theta - \tau \quad (6)$$

$$\theta^* = \theta + \tau \quad (7)$$

$$\vec{n} = (n_1, n_2, n_3) = \frac{\vec{s}\,\sin\theta' + \vec{t}\,\sin\theta^*}{\sin(2\theta)}. \quad (8)$$

Eq. (8) for the mirror-center normal vector has a singularity due to the zero denominator when the nominal incident angle $\theta = 0°$. Hence, this paper presents a more useful expression for the sun-tracking mirror normal. Following Eq. (8), the general azimuth–elevation tracking angle formula is denoted by operator Γ_{az-el} as:

$$(\gamma, \alpha) = \Gamma_{az-el}(\vec{n} = (n_1, n_2, n_3), \psi_a, \psi_t, \tau_1, \mu) \quad (9)$$

Guo et al. (2011) gave Eq. (9) as:

$$a_{11} = \cos\psi_t \cos^2\psi_a + \sin^2\psi_a, \quad (10)$$

$$a_{12} = (\cos\psi_t - 1)\sin\psi_a \cos\psi_a, \quad (11)$$

$$a_{13} = -\sin\psi_t \cos\psi_a, \quad (12)$$

$$a_{22} = \cos^2\psi_a + \cos\psi_t \sin^2\psi_a, \quad (13)$$

$$a_{23} = -\sin\psi_t \sin\psi_a, \tag{14}$$

$$a_{33} = \cos\psi_t, \tag{15}$$

$$c_1 = n_1 a_{11} + n_2 a_{12} + n_3 a_{13}, \tag{16}$$

$$c_2 = n_1 a_{12} + n_2 a_{22} + n_3 a_{23}, \tag{17}$$

$$c_3 = -n_1 a_{13} - n_2 a_{23} + n_3 a_{33}, \tag{18}$$

$$\alpha = \sin^{-1}((c_3 - \sin\tau_1 \sin\mu)/(\cos\tau_1 \cos\mu)), \tag{19}$$

$$d_1 = \cos\mu \cos\alpha, \tag{20}$$

$$d_2 = \cos\tau_1 \sin\mu - \sin\tau_1 \cos\mu \sin\alpha, \tag{21}$$

$$\begin{cases} \gamma = \cos^{-1}\{(\mathbf{c}_1\mathbf{d}_1 + \mathbf{c}_2\mathbf{d}_2)/(\mathbf{c}_1^2 + \mathbf{c}_2^2)\}, if(\mathbf{c}_2\mathbf{d}_1 - \mathbf{c}_1\mathbf{d}_2) \geqslant 0 \\ \gamma = 360^\circ - \cos^{-1}\{(\mathbf{c}_1\mathbf{d}_1 + \mathbf{c}_2\mathbf{d}_2)/(\mathbf{c}_1^2 + \mathbf{c}_2^2)\}, if(\mathbf{c}_2\mathbf{d}_1 - \mathbf{c}_1\mathbf{d}_2) < 0 \end{cases} \tag{22}$$

Each angular parameter in Eq. (9) has a period of 360°. Other key properties of the six angular parameters (ψ_a, ψ_t, γ, τ_1, α, μ) of Eq. (9) will be discussed in this paper. The six angular error parameters (ψ_a, ψ_t, γ_0, τ_1, α_0, μ) can be determined from experimental tracking data using a least squares fit for a specific azimuth–elevation tracking heliostat (Guo et al., 2012). The values of (ψ_a, ψ_t, γ_0, τ_1, α_0, μ) can then be post-regulated within the expected range using the properties of Eq. (9). Here, α_0 is the zero angle positioning error of the elevation axis and γ_0 is the zero angle positioning error of the azimuth axis. The geometric definition of γ_0 illustrated in Fig. 2 is similar to the definition of α_0.

The elevation rotation of an azimuth–elevation tracking heliostat is normally actuated by a set of electric drive screws, so the geometric relationship between the elevation tracking angle, α, and the linear motion, x, of the screw actuator shown in Fig. 3 will also be given.

Open-loop tracking control is usually used with heliostats in solar tower systems with a beam characterization system (BCS) (King, 1982; Strachan, 1993; Berenguel et al., 2004) often used to identify the image centers on the heliostat target plane so that measured tracking data can be used to evaluate the heliostat tracking errors around the aim point direction. However, measured tracking data is rarely used to evaluate the single axis tracking accuracy of dual-axis tracking heliostats. This paper gives a mathematical approach to evaluate the tracking accuracy of each heliostat axis using the general azimuth–elevation tracking angle formula based on measured tracking data.

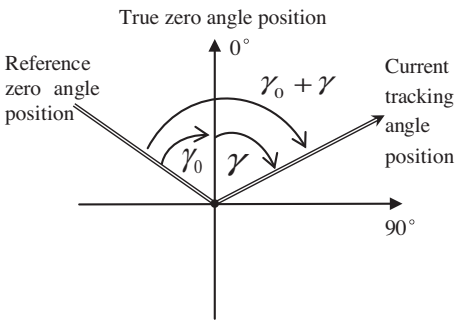

Fig. 2. Schematic diagram of the zero angle positioning error, γ_0, of the azimuth axis. The zero angle positioning error is defined as the angular difference between the true zero angle positioning and the reference zero angle positioning of the rotational axis.

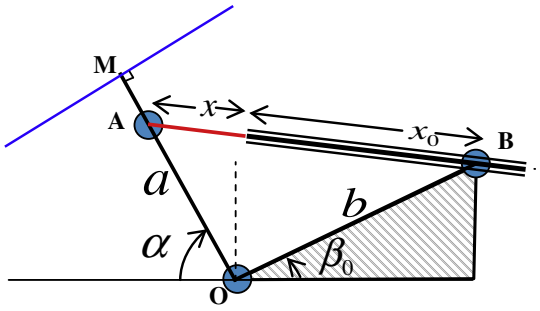

Fig. 3. Elevation rotation geometry of a heliostat with linear screw motion x corresponding to the elevation tracking angle α. The elevation axis is perpendicular to the plane of the figure with point **O** standing for the heliostat pivot and point **M** standing for the mirror surface center. The elevation of the mirror surface normal is driven by the linear screw actuator with length x_0 which limits the motion of pivot **A**. Points **O** and **B** are fixed pivots with line **OB** having slope β_0. The length of line **OA** is a, the length of line **OB** is b, and the length of line **AB** is $x + x_0$.

2. Robust expression for the mirror-surface-center normal

A robust expression for the mirror normal is very important for the general azimuth–elevation tracking angle formula given in Eq. (9). Although Eq. (8) gives the accurate mirror normal at the mirror surface center for a normal tracking heliostat with a mirror-pivot offset, Eq. (8) is singular for $\theta = 0°$ when the sun, the aim point, the mirror surface center and the heliostat pivot are in one line so that the mirror-surface-center normal coincides with the solar vector and the aim point vector, i.e. $\vec{n} = \vec{s} = \vec{t}$. This paper presents a more robust expression for the mirror normal that eliminates the singularity for $\theta = 0°$.

Eq. (8) can be rewritten as:

$$\begin{aligned} \vec{n} &= \frac{\vec{s}\,\sin\theta' + \vec{t}\,\sin\theta^*}{\sin(2\theta)} \\ &= \frac{\vec{s}\,\sin(\theta-\tau) + \vec{t}\,\sin(\theta+\tau)}{\sin(2\theta)} \\ &= \frac{\vec{s}(\sin\theta\cos\tau - \cos\theta\sin\tau) + \vec{t}(\sin\theta\cos\tau + \cos\theta\sin\tau)}{2\sin\theta\cos\theta} \\ &= \frac{\sin\theta\cos\tau(\vec{s}+\vec{t}) - \cos\theta\sin\tau(\vec{s}-\vec{t})}{2\sin\theta\cos\theta} \\ &= \frac{\cos\tau}{\cos\theta}\cdot\frac{\vec{s}+\vec{t}}{2} + \frac{\sin\tau}{\sin\theta}\cdot\frac{\vec{t}-\vec{s}}{2} \end{aligned} \tag{23}$$

From Eq. (5),

$$\sin\tau = \frac{H_z \sin\theta}{2L - H_z\cos\theta} \tag{24}$$

$$\frac{\sin\tau}{\sin\theta} = \frac{H_z}{2L - H_z\cos\theta} \tag{25}$$

Substituting Eq. (25) into Eq. (23) yields:

$$\vec{n} = \frac{\cos\tau}{\cos\theta}\cdot\frac{\vec{s}+\vec{t}}{2} + \frac{H_z}{2L - H_z\cos\theta}\cdot\frac{\vec{t}-\vec{s}}{2}. \quad (26)$$

Eq. (26) is a robust mirror-center normal vector that is derived from Eq. (8) and is equivalent to Eq. (8), but is more numerically stable than Eq. (8). In the case of $\theta = 0°$, $\cos\theta = 1$, $\tau = 0°$, $\cos\tau = 1$ and $\vec{s} = \vec{t}$, so $\vec{n} = \vec{s} = \vec{t}$ and Eq. (26) still holds.The expressions for the robust mirror-center normal vector are then Eqs. (1)–(5), and (26), with these expressions denoted by operator Γ_{normal} as:

$$(n_1, n_2, n_3) = \Gamma_{normal,1}(\mathbf{OT} = (t_1, t_2, t_3), \gamma_s, \alpha_s, H_z). \quad (27)$$

The complete general azimuth–elevation tracking angle formula is composed of Eqs. (27) and (9). For convenience, this general azimuth–elevation tracking angle formula is denoted by the mathematical operator, Γ:

$$(\gamma, \alpha) = \Gamma(\mathbf{OT} = (t_1, t_2, t_3), \gamma_s, \alpha_s, H_z, \psi_a, \psi_t, \tau_1, \mu). \quad (28)$$

3. Parametric properties of the general azimuth–elevation tracking angle formula

This section gives some important properties of Eq. (9) related to the six angular parameters (ψ_a, ψ_t, γ, τ_1, α, μ). The nine angular properties (Eqs. (31)–(37), (39), and (40)) of this tracking angle formula are useful for readers to further understand the general tracking geometry for an azimuth–elevation tracking heliostat with typical geometric errors. More important, since the least squares fit used to determine the six angular error parameters (ψ_a, ψ_t, γ_0, τ_1, α_0, μ) from experimental tracking data for a specific heliostat uses an unconstrained optimization method (Guo et al., 2012) and SINCE different initial parameters and searching strategies can lead to different but equivalent solutions, the values of (ψ_a, ψ_t, γ_0, τ_1, α_0, μ) can then be regulated within the expected range using the angular properties of Eq. (9). Here, α_0 is the zero angle positioning error of the elevation axis and γ_0 is the zero angle positioning error of the azimuth axis. α_0 and γ_0 can be treated in the same way as α and γ when using the properties of Eq. (9) in this section. For example, γ_0, ψ_t and ψ_a are shifted into the desired range of 0–360°, and α_0, μ and τ_1 are shifted into in the range of −90–90°. The equivalent solutions should share the identical mirror-surface-center normal. Although the regressed values of (ψ_a, ψ_t, γ_0, τ_1, α_0, μ) without post-regulation can be directly used in the general azimuth–elevation tracking angle formula, the post-regulated angular parameters have more clear physical meanings.

According to Guo et al. (2011), Eq. (9) is equivalent to:

$$\begin{aligned}\vec{n} &= (n_1, n_2, n_3)\\ &= (\cos\mu, \sin\mu, 0)B_6(\alpha)B_5(\tau_1)B_4(\gamma)B_3(\psi_a)B_2(\psi_t)B_1(\psi_a).\end{aligned} \quad (29)$$

Here, $B_1(\psi_a)$, $B_2(\psi_t)$, $B_3(\psi_a)$, $B_4(\gamma)$, $B_5(\tau_1)$ and $B_6(\alpha)$ are the six rotational transformation matrices defined as:

$$B_1(\psi_a) = \begin{bmatrix} \cos\psi_a & \sin\psi_a & 0 \\ -\sin\psi_a & \cos\psi_a & 0 \\ 0 & 0 & 1 \end{bmatrix},$$

$$B_2(\psi_t) = \begin{bmatrix} \cos\psi_t & 0 & -\sin\psi_t \\ 0 & 1 & 0 \\ \sin\psi_t & 0 & \cos\psi_t \end{bmatrix},$$

$$B_3(\psi_a) = \begin{bmatrix} \cos\psi_a & -\sin\psi_a & 0 \\ \sin\psi_a & \cos\psi_a & 0 \\ 0 & 0 & 1 \end{bmatrix},$$

$$B_4(\gamma) = \begin{bmatrix} \cos\gamma & \sin\gamma & 0 \\ -\sin\gamma & \cos\gamma & 0 \\ 0 & 0 & 1 \end{bmatrix},$$

$$B_5(\tau_1) = \begin{bmatrix} 1 & 0 & 0 \\ 0 & \cos\tau_1 & \sin\tau_1 \\ 0 & -\sin\tau_1 & \cos\tau_1 \end{bmatrix},$$

$$B_6(\alpha) = \begin{bmatrix} \cos\alpha & 0 & \sin\alpha \\ 0 & 1 & 0 \\ -\sin\alpha & 0 & \cos\alpha \end{bmatrix}.$$

Thus, Eq. (29) can be used to analyze the parametric properties of the angles in the general azimuth–elevation tracking angle formula. For convenience, Eq. (29) is denoted here as:

$$(n_1, n_2, n_3) = \Gamma_{normal,2}(\psi_a, \psi_t, \gamma, \tau_1, \alpha, \mu). \quad (30)$$

3.1. Periodicity of 360° for each angular parameter

The following equations hold from Eqs. (29) and (30):

$$\Gamma_{normal,2}(\psi_a, \psi_t, \gamma, \tau_1, \alpha, \mu) = \Gamma_{normal,2}(\psi_a \pm 360^\circ, \psi_t, \gamma, \tau_1, \alpha, \mu) \quad (31)$$

$$\Gamma_{normal,2}(\psi_a, \psi_t, \gamma, \tau_1, \alpha, \mu) = \Gamma_{normal,2}(\psi_a, \psi_t \pm 360^\circ, \gamma, \tau_1, \alpha, \mu) \quad (32)$$

$$\Gamma_{normal,2}(\psi_a, \psi_t, \gamma, \tau_1, \alpha, \mu) = \Gamma_{normal,2}(\psi_a, \psi_t, \gamma \pm 360^\circ, \tau_1, \alpha, \mu) \quad (33)$$

$$\Gamma_{normal,2}(\psi_a, \psi_t, \gamma, \tau_1, \alpha, \mu) = \Gamma_{normal,2}(\psi_a, \psi_t, \gamma, \tau_1 \pm 360^\circ, \alpha, \mu) \quad (34)$$

$$\Gamma_{normal,2}(\psi_a, \psi_t, \gamma, \tau_1, \alpha, \mu) = \Gamma_{normal,2}(\psi_a, \psi_t, \gamma, \tau_1, \alpha \pm 360^\circ, \mu) \quad (35)$$

$$\Gamma_{normal,2}(\psi_a, \psi_t, \gamma, \tau_1, \alpha, \mu) = \Gamma_{normal,2}(\psi_a, \psi_t, \gamma, \tau_1, \alpha, \mu \pm 360^\circ) \quad (36)$$

3.2. Correlation between ψ_a and ψ_t

The following equation also holds from Eqs. (29) and (30):

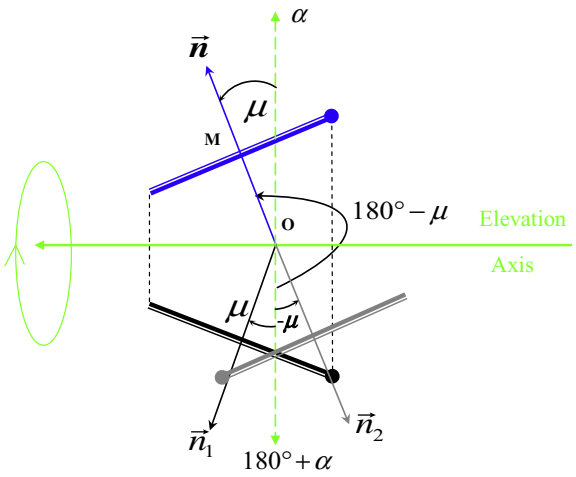

Fig. 4. Symmetric nature of the heliostat tracking geometry for Eq. (39). Parameter sets (α, μ) and $(\alpha + 180°, 180° - \mu)$ with the other four angular parameters being the same give the same mirror normal.

$$\Gamma_{normal,2}(\psi_a, \psi_t, \gamma, \tau_1, \alpha, \mu) = \Gamma_{normal,2}(\psi_a + 180^\circ, -\psi_t, \gamma, \tau_1, \alpha, \mu). \quad (37)$$

The mathematical proof is given as:

$$B_3(\psi_a)B_2(\psi_t)B_1(\psi_a) = \begin{bmatrix} a_{1,1}(\psi_a,\psi_t) & a_{1,2}(\psi_a,\psi_t) & a_{1,3}(\psi_a,\psi_t) \\ -a_{1,2}(\psi_a,\psi_t) & a_{2,2}(\psi_a,\psi_t) & a_{2,3}(\psi_a,\psi_t) \\ -a_{1,3}(\psi_a,\psi_t) & -a_{2,3}(\psi_a,\psi_t) & a_{3,3}(\psi_a,\psi_t) \end{bmatrix},$$

$$a_{1,1}(\psi_a,\psi_t) = \cos\psi_t \cos^2\psi_a + \sin^2\psi_a,$$
$$a_{1,2}(\psi_a,\psi_t) = (\cos\psi_t - 1)\sin\psi_a \cos\psi_a,$$
$$a_{1,3}(\psi_a,\psi_t) = -\sin\psi_t \cos\psi_a,$$
$$a_{2,2}(\psi_a,\psi_t) = \cos^2\psi_a + \cos\psi_t \sin^2\psi_a,$$
$$a_{2,3}(\psi_a,\psi_t) = -\sin\psi_t \sin\psi_a,$$
$$a_{3,3}(\psi_a,\psi_t) = \cos\psi_t,$$

Then,
$a_{i,j}(\psi_a,\psi_t) = a_{i,j}(\psi_a + 180^\circ, -\psi_t), i = 1,2,3; j = i,\cdots,3,$
and

$$B_3(\psi_a)B_2(\psi_t)B_1(\psi_a) = B_3(\psi_a + 180^\circ)B_2(-\psi_t)B_1(\psi_a + 180^\circ). \quad (38)$$

Thus, the following holds by using Eq. (38).

$$\begin{aligned}&\Gamma_{normal,2}(\psi_a + 180^\circ, -\psi_t, \gamma, \tau_1, \alpha, \mu)\\ &= [(\cos\mu, \sin\mu, 0)B_6(\alpha)B_5(\tau_1)B_4(\gamma)][B_3(\psi_a + 180^\circ)B_2(-\psi_t)B_1(\psi_a + 180^\circ)]\\ &= [(\cos\mu, \sin\mu, 0)B_6(\alpha)B_5(\tau_1)B_4(\gamma)][B_3(\psi_a)B_2(\psi_t)B_1(\psi_a)]\\ &= \Gamma_{normal,2}(\psi_a, \psi_t, \gamma, \tau_1, \alpha, \mu).\end{aligned}$$

Eq. (37) means that the azimuth axis tilting expressions (ψ_a, ψ_t) and $(\psi_a + 180°, -\psi_t)$ have the same azimuth-axis pointing direction. The azimuth axis tilted a positive tilt angle in an azimuth direction can also be described by tilts a negative tilt angle relative to the opposite azimuth direction. For example, an azimuth axis tilt of 1 mrad to the west can also be understood to tilt −1 mrad to the east. So the mirror normal is same.

3.3. Correlation between μ and α

The following equation also holds from Eqs. (29) and (30):

$$\Gamma_{normal,2}(\psi_a, \psi_t, \gamma, \tau_1, \alpha, \mu) = \Gamma_{normal,2}(\psi_a, \psi_t, \gamma, \tau_1, \alpha + 180^\circ, 180^\circ - \mu). \quad (39)$$

The mathematical proof is given as:

$$\begin{aligned}&(\cos\mu, \sin\mu, 0)B_6(\alpha) = (\cos\mu\cos\alpha, \sin\mu, \cos\mu\sin\alpha)\\ &= (-\cos\mu\cos(\alpha + 180^\circ), \sin\mu, -\cos\mu\sin(\alpha + 180^\circ))\\ &= (\cos(180^\circ - \mu)\cos(\alpha + 180^\circ), \sin(180^\circ - \mu),\\ &\quad \cos(180^\circ - \mu)\sin(\alpha + 180^\circ))\\ &= (\cos(180^\circ - \mu), \sin(180^\circ - \mu), 0)B_6(\alpha + 180^\circ)\end{aligned}$$

Thus,

$$\begin{aligned}&\Gamma_{normal,2}(\psi_a, \psi_t, \gamma, \tau_1, \alpha, \mu)\\ &= [(\cos\mu, \sin\mu, 0)B_6(\alpha)][B_5(\tau_1)B_4(\gamma)B_3(\psi_a)B_2(\psi_t)B_1(\psi_a)]\\ &= [(\cos(180^\circ - \mu), \sin(180^\circ - \mu), 0)B_6(\alpha + 180^\circ)]\\ &\quad [B_5(\tau_1)B_4(\gamma)B_3(\psi_a)B_2(\psi_t)B_1(\psi_a)]\\ &= \Gamma_{normal,2}(\psi_a, \psi_t, \gamma, \tau_1, \alpha + 180^\circ, 180^\circ - \mu).\end{aligned}$$

Eq. (39) means that the parameter sets (α, μ) and $(\alpha + 180^\circ, 180^\circ - \mu)$ with the other four angular parameters being the same give the same mirror normal. Following Figs. 1 and 4 illustrate the symmetric nature of the heliostat tracking geometry for Eq. (39). In Fig. 4, the mirror surface rotates around the elevation axis from position α to α + 180°, the parameter set (α, μ) is for the mirror-surface-center normal, $\vec{n}$, $(\alpha + 180°, \mu)$ is for the mirror-surface-center normal, $\vec{n}_1$, $(\alpha + 180°, -\mu)$ is for the mirror-surface-center normal, $\vec{n}_2$, and $(\alpha + 180°, 180° - \mu)$ gives the same mirror-surface-center normal as (α, μ). $\vec{n}$, $\vec{n}_1$ and $\vec{n}_2$ are in a plane with $\vec{n}$ and $\vec{n}_1$ symmetric about the elevation axis and $\vec{n}_1$ and $\vec{n}_2$ symmetric about the α + 180° line.

3.4. Correlation between γ, τ1 and α

The following equation also holds from Eqs. (29) and (30):

$$\Gamma_{normal,2}(\psi_a, \psi_t, \gamma, \tau_1, \alpha, \mu) = \Gamma_{normal,2}(\psi_a, \psi_t, \gamma + 180^\circ, 180^\circ - \tau_1, \alpha + 180^\circ, \mu). \quad (40)$$

The mathematical proof is given as:

$$B_6(\alpha)B_5(\tau_1)B_4(\gamma)=\begin{bmatrix} b_{1,1}(\gamma,\tau_1,\alpha) & b_{1,2}(\gamma,\tau_1,\alpha) & b_{1,3}(\gamma,\tau_1,\alpha)\\ b_{2,1}(\gamma,\tau_1,\alpha) & b_{2,2}(\gamma,\tau_1,\alpha) & b_{2,3}(\gamma,\tau_1,\alpha)\\ b_{3,1}(\gamma,\tau_1,\alpha) & b_{3,2}(\gamma,\tau_1,\alpha) & b_{3,3}(\gamma,\tau_1,\alpha)\end{bmatrix}$$

$$=\begin{bmatrix} \cos\alpha\cos\gamma+\sin\alpha\sin\gamma\sin\tau_1 & \cos\alpha\sin\gamma-\sin\alpha\cos\gamma\sin\tau_1 & \sin\alpha\cos\tau_1\\ -\cos\tau_1\sin\gamma & \cos\tau_1\cos\gamma & \sin\tau_1\\ -\sin\alpha\cos\gamma+\cos\alpha\sin\gamma\sin\tau_1 & -\sin\alpha\sin\gamma-\cos\alpha\cos\gamma\sin\tau_1 & \cos\alpha\cos\tau_1\end{bmatrix}$$

$$\begin{aligned} b_{1,1}(\gamma,\tau_1,\alpha)&=\cos\alpha\cos\gamma+\sin\alpha\sin\gamma\sin\tau_1\\ &=(-\cos\alpha)(-\cos\gamma)+(-\sin\alpha)(-\sin\gamma)\sin\tau_1\\ &=\cos(\alpha+180^\circ)\cos(\gamma+180^\circ)+\sin(\alpha+180^\circ)\sin(\gamma+180^\circ)\sin(180^\circ-\tau_1)\\ &=b_{1,1}(\gamma+180^\circ,180^\circ-\tau_1,\alpha+180^\circ)\\ b_{1,2}(\gamma,\tau_1,\alpha)&\\ &=\cos\alpha\sin\gamma-\sin\alpha\cos\gamma\sin\tau_1\\ &=(-\cos\alpha)(-\sin\gamma)-(-\sin\alpha)(-\cos\gamma)\sin\tau_1\\ &=\cos(\alpha+180^\circ)\sin(\gamma+180^\circ)-\sin(\alpha+180^\circ)\cos(\gamma+180^\circ)\sin(180^\circ-\tau_1)\\ &=b_{1,2}(\gamma+180^\circ,180^\circ-\tau_1,\alpha+180^\circ)\end{aligned}$$

$$\begin{aligned} b_{1,3}(\gamma,\tau_1,\alpha)&=\sin\alpha\cos\tau_1=(-\sin\alpha)(-\cos\tau_1)\\ &=\sin(\alpha+180^\circ)\cos(180^\circ-\tau_1)\\ &=b_{1,3}(\gamma+180^\circ,180^\circ-\tau_1,\alpha+180^\circ)\\ b_{2,1}(\gamma,\tau_1,\alpha)&=-\cos\tau_1\sin\gamma=-(-\cos\tau_1)(-\sin\gamma)\\ &=-\cos(180^\circ-\tau_1)\sin(\gamma+180^\circ)\\ &=b_{2,1}(\gamma+180^\circ,180^\circ-\tau_1,\alpha+180^\circ)\\ b_{2,2}(\gamma,\tau_1,\alpha)&=\cos\tau_1\cos\gamma=(-\cos\tau_1)(-\cos\gamma)\\ &=\cos(180^\circ-\tau_1)\cos(\gamma+180^\circ)\\ &=b_{2,2}(\gamma+180^\circ,180^\circ-\tau_1,\alpha+180^\circ)\\ b_{2,3}(\gamma,\tau_1,\alpha)&=\sin\tau_1\\ &=\sin(180^\circ-\tau_1)=b_{2,3}(\gamma+180^\circ,180^\circ-\tau_1,\alpha+180^\circ)\\ b_{3,1}(\gamma,\tau_1,\alpha)&\\ &=-\sin\alpha\cos\gamma+\cos\alpha\sin\gamma\sin\tau_1\\ &=-(-\sin\alpha)(-\cos\gamma)+(-\cos\alpha)(-\sin\gamma)\sin\tau_1\\ &=-\sin(\alpha+180^\circ)\cos(\gamma+180^\circ)+\cos(\alpha+180^\circ)\\ &\quad\sin(\gamma+180^\circ)\sin(180^\circ-\tau_1)\\ &=b_{3,1}(\gamma+180^\circ,180^\circ-\tau_1,\alpha+180^\circ)\\ b_{3,2}(\gamma,\tau_1,\alpha)&=-\sin\alpha\sin\gamma-\cos\alpha\cos\gamma\sin\tau_1\\ &=-(-\sin\alpha)(-\sin\gamma)-(-\cos\alpha)(-\cos\gamma)\sin\tau_1\\ &=-\sin(\alpha+180^\circ)\sin(\gamma+180^\circ)-\cos(\alpha+180^\circ)\\ &\quad\cos(\gamma+180^\circ)\sin(180^\circ-\tau_1)\\ &=b_{3,2}(\gamma+180^\circ,180^\circ-\tau_1,\alpha+180^\circ)\\ b_{3,3}(\gamma,\tau_1,\alpha)&\\ &=\cos\alpha\cos\tau_1\\ &=(-\cos\alpha)(-\cos\tau_1)\\ &=\cos(\alpha+180^\circ)\cos(180^\circ-\tau_1)\\ &=b_{3,3}(\gamma+180^\circ,180^\circ-\tau_1,\alpha+180^\circ)\end{aligned}$$

So $b_{i,j}(\gamma,\tau_1,\alpha)=b_{i,j}(\gamma+180^\circ,180^\circ-\tau_1,\alpha+180^\circ), i=1,2,3; j=1,2,3.$, i.e., $B_6(\alpha)B_5(\tau_1)B_4(\gamma)=B_6(\alpha+180^\circ)B_5(180^\circ-\tau_1)\ B_4(\gamma+180°)$.

Thus,

$\Gamma_{normal,2}(\psi_a,\psi_t,\gamma,\tau_1,\alpha,\mu)=(\cos\mu,\sin\mu,0)$ $[B_6(\alpha)\ B_5(\tau_1)\ B_4(\gamma)][B_3(\psi_a)\ B_2(\psi_t)\ B_1(\psi_a)]=(\cos\mu,\sin\mu,0)$ $[B_6(\alpha+180°)\ B_5(180°-\tau_1)\ B_4(\gamma+180°)][B_3(\psi_a)\ B_2(\psi_t)\ B_1(\psi_a)]=\Gamma_{normal,2}(\psi_a,\psi_t,\gamma+180°,180°-\tau_1,\alpha+180°,\mu)$.

Eq. (40) means that the parameter sets (γ,τ_1,α) and $(\gamma+180^\circ,180^\circ-\tau_1,\alpha+180^\circ)$ with the other three angular parameters being the same give the same mirror normal, $\vec{n}$. Following Fig. 1, Fig. 5 illustrates the three-dimensional symmetric nature of the heliostat tracking geometry for Eq. (40). In Fig. 5, plane Π_1 is determined by the two rotational axes, it rotates around the azimuth axis, and the normal of Π_1 corresponds to the azimuth tracking angle γ. Plane Π_2 with an elevation tracking angle α is determined by the elevation axis and the mirror-surface-center normal, $\vec{n}$, also rotates around the azimuth axis together with the dual-axis plane Π_1. Plane Π_3 is marked by the red dotted boundary lines and plane Π_4 is marked by the blue dashed-and-dotted boundary lines. Π_3 and Π_4 are two three-dimensional symmetric positions of Π_2. The sweeping moment of the elevation axis around the azimuth axis gives a conical surface due to the fixed dual-axis non-orthogonal angle, τ_1. (γ,τ_1,α) is for the mirror-surface-center normal, $\vec{n}$, and $(\gamma+180^\circ,\tau_1,\alpha)$ and $(\gamma+180^\circ,180^\circ-\tau_1,\alpha)$ are for the new mirror normal positions $\vec{n}_3$ and $\vec{n}_4$. When the heliostat turns 180° around the azimuth axis, Π_1 is orientated in the opposite direction with the azimuth tracking angle $\gamma+180°$, Π_2 turns to Π_3 with the elevation tracking angle α being unchanged, and $\vec{n}$ moves to $\vec{n}_3$. Then, let plane Π_3 together with the elevation axis turn around the normal line of plane Π_1 for $180^\circ-2\tau_1$ (from angular position τ_1 to $180^\circ-\tau_1$) with the elevation tracking angle still being α. Thus, plane Π_3 moves to Π_4, the elevation axis returns to the original direction from the position of $\gamma+180°$, and the mirror-surface-center normal turns to $\vec{n}_4$. In this case, plane Π_4 is symmetric and parallel to plane Π_2, and $\vec{n}_4$ and $\vec{n}$ are in a plane and are symmetric about the elevation axis. Therefore, mirror normal $\vec{n}_4$ returns exactly back to $\vec{n}$

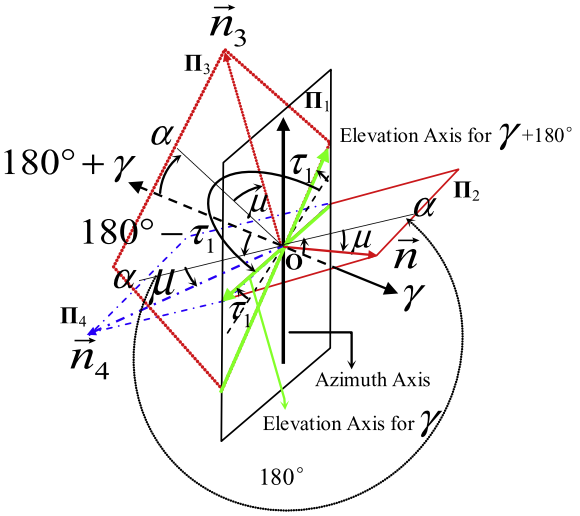

Fig. 5. Three-dimensional symmetric nature of the heliostat tracking geometry for Eq. (40). Parameter sets (γ,τ_1,α) and $(\gamma+180°,180°-\tau_1,\alpha+180°)$ with the other three angular parameters being same give the same mirror normal.

when the heliostat further rotates 180° around the elevation axis with the azimuth tracking angle of $\gamma + 180°$ being unchanged.

4. Geometric relationship between the elevation tracking angle, α, and the linear screw motion, x

Fig. 3 illustrates the elevation rotation geometry of an azimuth–elevation tracking heliostat with a screw elevation actuator. The elevation tracking angle, α, is related to the linear motion, x, of the screw actuator. In Fig. 3, the elevation axis is perpendicular to the plane of the figure with point **O** standing for the heliostat pivot and point **M** standing for the mirror surface center. The elevation of the mirror surface normal is driven by the linear screw actuator with length x_0 which limits the rotation of the moving pivot **A**. Points **O** and **B** are fixed pivots with line **OB** having a slope angle of β_0. The length of line **OA** is a, the length of line **OB** is b, and the length of line **AB** is $x + x_0$.

According to the law of cosines, the length of side **AB** of triangle **OAB** is given by:

$$\begin{aligned} x + x_0 &= (a^2 + b^2 - 2ab\cos(\angle AOB))^{0.5} \\ &= (a^2 + b^2 - 2ab\cos(180^\circ - \alpha - \beta_0))^{0.5} \\ &= (a^2 + b^2 + 2ab\cos(\alpha + \beta_0))^{0.5} \end{aligned}$$

So

$$x = (a^2 + b^2 + 2ab\cos(\alpha + \beta_0))^{0.5} - x_0. \tag{41}$$

From Eq. (41), the elevation tracking angle, α, is:

$$\alpha = \cos^{-1}\left(\frac{(x + x_0)^2 - (a^2 + b^2)}{2ab}\right) - \beta_0. \tag{42}$$

Eq. (41) gives an expression for x as a function of α, while Eq. (42) gives an expression for α as a function of x.

5. Approach for evaluating the tracking accuracy of each heliostat axis from measured tracking data

This section gives a practical approach for evaluating the tracking accuracy of each heliostat axis from experimental tracking data using the general azimuth–elevation tracking angle formula in Eq. (28). This approach can also be used to determine the heliostat zero angle positioning errors of the two rotational axes.

Assume a set of sun tracking test data for the azimuth–elevation tracking angle formula with known geometric parameters (ψ_a, ψ_t, τ_1, μ, H_z) with:

- solar position angles: α_s^i and γ_s^i, $i = 1, 2, \ldots, q$.
- measured azimuth–elevation tracking angles: γ_i' and α_i', $i = 1, 2, \cdots, q$.
- sun beam reflection points on the target plane in the coordinate system [**O**; North, East, Height]:

$$\mathrm{OT}_i = (t_1^i, t_2^i, t_3^i), i = 1, 2, \ldots q.$$

where q is the number of heliostat tracking points.

The computed tracking angles from the experimental tracking data using Eq. (28) are:

$$(\gamma_i, \alpha_i) = \Gamma(\mathbf{OT}_i = (t_1^i, t_2^i, t_3^i), \gamma_s^i, \alpha_s^i, H_z, \psi_a, \psi_t, \tau_1, \mu), \quad i = 1, 2, \cdots, q. \tag{43}$$

The mean and the standard deviation of the differences between the measured and the computed azimuth tracking angles are then:

$$\gamma_0 = \sum_{i=1}^{q}(\gamma_i' - \gamma_i)/q \tag{44}$$

$$\sigma_\gamma = \sqrt{\sum_{i=1}^{q}(\gamma_i' - \gamma_i - \gamma_0)^2/(q-1)}. \tag{45}$$

The mean and the standard deviation of the differences between the measured and the computed elevation tracking angles are

$$\alpha_0 = \sum_{i=1}^{q}(\alpha_i' - \alpha_i)/q \tag{46}$$

$$\sigma_\alpha = \sqrt{\sum_{i=1}^{q}(\alpha_i' - \alpha_i - \alpha_0)^2/(q-1)}. \tag{47}$$

σ_γ and σ_α are useful indexes for seperately evaluating the tracking precisions of the azimuth axis and the elevation axis for the heliostat from measured data. The parameters γ_0 and α_0 are good estimates of the real zero angle positioning errors of the azimuth axis and the elevation axis.

Guo et al. (2011) reported on the use of nine laser beam tracking tests on a specially designed heliostat model with $\psi_t = 1.854°$, $\psi_a = 236.06°$, $\tau_1 = 5°$ and $\mu = -0.92°$. The data gave $\gamma_0 = -237.43°$, $\sigma_\gamma = 0.014°$, $\alpha_0 = 22.832°$ and $\sigma_\alpha = 0.011°$ using Eqs. (44)–(47). Since $\sigma_\gamma = 0.014°$ and $\sigma_\alpha = 0.011°$ are quite small considering the experimental conditions, the general tracking angle formula is shown to be quite accurate and the tracking accuracies of the two heliostat axes are high.

6. Conclusions

The general azimuth–elevation tracking angle formula for a heliostat with a mirror-pivot offset and other angular errors developed earlier is re-rewritten here as a series of easily solved expressions. The original expression for the tracking mirror normal vector in the tracking angle formula is singular when the nominal incident angle is zero. A numerically stable expression for the mirror normal vector is given here. Some important properties of this tracking angle formula about the six angular parameters (ψ_a, ψ_t, γ, τ_1, α, μ) are discussed for regulating these angular parameters within expected ranges for heliostat tracking. This paper also gives expressions relating the elevation tracking angle to the linear motion of the elevation

screw actuator of a heliostat to facilitate use of the general azimuth–elevation tracking angle formula in heliostat designs. A practical approach is then given to evaluate the tracking precision of each heliostat rotational axis from experimental data using the general tracking angle formula. This approach can also be used to determine the heliostat zero angle positioning errors of the two rotational axes.

Acknowledgements

This work was supported by the National Natural Science Foundation of China (No. 50906078), the National Basic Research Program of China (No. 2010CB227106), and the China National Hi-Tech R&D (863 Plan) project: Study on the system of the solar concentration and heat absorption for a solar tower power plant (No. 2013AA050502). We thank Lorin Vant-Hull for his helpful comments on the paper before submission.

References

Baheti, R.S., Scott, P.F., 1980. Design of self-calibrating controllers for heliostats in a solar power plant. IEEE Trans. Autom. Control AC-25 (6), 1091–1097.

Berenguel, M., Rubio, F.R., Valverde, A., Lara, P.J., Arahal, M.R., Camacho, E.F., Lopez, M., 2004. An artificial vision-based control system for automatic heliostat positioning offset correction in a central receiver solar power plant. Solar Energy 76 (5), 563–575.

Chong, K., Wong, C., 2009. General formula for on-axis sun-tracking system and its application in improving tracking accuracy of solar collector. Solar Energy 83 (3), 298–305.

Duffie, J.A., Beckman, W.A., 1991. Solar Engineering of Thermal Processes. John Wiley, New York, ISBN 0471510564.

Guo, M., Wang, Z., Liang, W., Zhang, X., Zang, C., Lu, Z., We, X., 2010. Tracking formulas and strategies for a receiver oriented dual-axis tracking toroidal heliostat. Solar Energy 84 (6), 939–947.

Guo, M., Wang, Z., Zhang, J., Sun, F., Zhang, X., 2011. Accurate altitude–azimuth tracking angle formulas for a heliostat with mirror-pivot offset and other fixed geometrical errors. Solar Energy 85 (5), 1091–1100.

Guo, M., Wang, Z., Zhang, J., Sun, F., Zhang, X., 2012. Determination of the angular parameters in the general altitude–azimuth tracking angle formulas for a heliostat with a mirror-pivot offset based on experimental tracking data. Solar Energy 86 (3), 941–950.

Khalsa, S.S.S., Ho, C.K., Andraka, C.E., 2011. An automated method to correct heliostat tracking errors. SolarPACES 2011, Granada, Spain, September 20–23, 2011.

King, D.L., 1982. Beam quality and tracking accuracy evaluation of second generation and barstow production heliostats. SAND82-0181, Sandia National Laboratories, Albuquerque, New Mexico, 1982.

Lipps, F.W., Vant-Hull, L.L., 1978. A cellwise method for solar central receivers systems. Solar Energy 20 (6), 505–516.

Mavis, C.L., 1988. 10 MWe Solar thermal central receiver pilot plant heliostat and beam characterization system evaluation. Tech. Rep. SAND87-8003, Sandia National Laboratories, Livermore (CA), 1988.

Stone, K.W., 1986. Automatic Heliostat Track Alignment Method. United States Patent No. 4,564,275, January 14, 1986.

Stone, K.W., Jones, S.A., 1999. Analysis of solar two heliostat tracking error sources. Tech. Rep. SAND99-0239c, Sandia National Laboratories, Albuquerque, New Mexico, 1999.

Strachan, J.W., 1993. Revisiting the BCS, a measurement system for characterizing the optics of solar collectors. In: 39th International Instrumentation Symposium, Albuquerque, New Mexico, 1993.